Deposition of a Thin Film of TiO_x from a Titanium Metal Target as Novel Blocking Layers at Conducting Glass/TiO_2 Interfaces in Ionic Liquid Mesoscopic TiO_2 Dye-Sensitized Solar Cells†

Jiangbin Xia, Naruhiko Masaki, Kejian Jiang, and Shozo Yanagida*

Center for Advanced Science and Innovation, Osaka University, Suita, Osaka 565-0871, Japan

Received: July 10, 2006; In Final Form: September 17, 2006

In dye-sensitized TiO_2 solar cells, charge recombination processes at interfaces between fluorine-doped tin oxide (FTO), TiO_2, dye, and electrolyte play an important role in limiting the photon-to-electron conversion efficiency. From this point of view, a high work function material such as titanium deposited by sputtering on FTO has been investigated as an effective blocking layer for preventing electron leakage from FTO without influencing electron injection. X-ray photoelectron spectroscopy analysis indicates that different species of Ti (Ti^{4+}, Ti^{3+}, Ti^{2+}, and a small amount of Ti^0) exist on FTO. Electrochemical and photoelectrochemical measurements reveal that thin films of titanium species, expressed as TiO_x, work as a compact blocking layer between FTO and TiO_2 nanocrystaline film, improving V_{oc} and the fill factor, finally giving a better conversion efficiency for dye-sensitized TiO_2 solar cells with ionic liquid electrolytes.

1. Introduction

In dye-sensitized TiO_2 solar cells (DSCs) that are composed of a dye-adsorbed nano-TiO_2 layer, fluorine-doped tin oxide (FTO) glass as the window electrode, electrolytes as the charge carrier, and a Pt counter electrode, unidirectional charge flow with no electron leakage at the interfaces is essential for high energy conversion efficiency. However, from the point of practical application, organic liquid electrolytes may not be a good choice because of their shortcomings such as the difficulty of sealing for evaporation and their instability at high temperatures. Much attention[1−4] has been paid recently to efforts to improve the performance of ionic liquid DSCs because of features of ionic liquids such as high ionic conductivity, nonvolatility, improved thermal stability, and nonflammability.[5−7]

Another kind of widely used conducting glass, indium−tin oxide (ITO), has attracted many researchers to take great efforts to modify its surface for higher performance in organic light-emitting diodes (OLEDs)[8] or organic solar cells.[9] For instance, a silanization reaction and formation[10,11] of self-assembled monolayers (SAMs)[12−14] are carried out to change the ITO electrode's work function. However, few groups pay attention to the modification of FTO in DSCs. One reason might be due to the necessary step of annealing the FTO/nano-TiO_2 electrode at a high temperature, which will damage the organic monolayer on FTO during the processes of the fabrication of the DSCs.

As to the DSC field, although some groups have studied the interface of FTO/TiO_2 mainly to establish some models[15−20] of DSCs or just to characterize[21,22] and investigate its effectiveness[23−28] by employing a compact TiO_2 layer, there is no intense investigation on this important interface in DSCs. However, suppression of electron leakage at the interface of FTO/TiO_2 plays an important role in the improvement of electron conversion efficiency, especially in the increase of the V_{oc} of the solar cells. Therefore, it is vital to attach importance to the interface of FTO/TiO_2 as emphasized by Professor L. M. Peter in his recent articles.[29−31] It should be noted that the blocking layer has a greater effect on the conversion efficiency in ionic liquid DSCs than that of organic liquid DSCs at 1 sun. In our previous study,[32,33] we found that a sputtering method might be the best way to form a blocking layer on FTO. Moreover, among different metal oxides examined, only Nb_2O_5 and TiO_2 show better performance. However, a TiO_2 blocking layer, also called a compact layer, formed by a spray pyrolysis method can improve cell performance.[24,25,32] Therefore, we need to reinvestigate this system from a practical point of view.

On the basis of this point, we continue to introduce other materials such as titanium due to its high work function properties as a potential barrier between the FTO and the nano-TiO_2 layer. Moreover, we expect that such a metal with good conductivity is favorable for injected electrons transporting to the external circuit. In earlier research Gregg et al.[17] and Rau et al.[34] have investigated some high work function materials such as Au, Al, Zn, Pt, or ITO as back-contact materials to probe the relationship between the work function of back-contact materials and the V_{oc}. Moreover, recently Zaban et al.[35] proposed a new structure using Ti/TiO_2 as a current collector due to the conductive properties of titanium in DSCs. However, they do not show any exciting results based on these different back-contact materials.

In this paper, a new FTO/TiO_x/mesoscopic TiO_2 electrode was fabricated, and its application in ionic liquid dye-sensitized solar cells was examined. Improvement should come from the TiO_x compact layer between the FTO and the mesoscopic TiO_2 layer, which will reduce the electron loss at the FTO/mesoscopic TiO_2 and FTO/ionic liquid electrolyte interfaces, leading to the increase of V_{oc} and the fill factor.

2. Experimental Section

Titanium-modified FTO substrates were fabricated by depositing Ti particles onto FTO (Nippon Sheet Glass, SnO_2:F,

† Part of the special issue "Arthur J. Nozik Festschrift".

* Author to whom correspondence should be addressed. Phone/Fax: +81-06-6879-7351. E-mail: yanagida@mls.eng.osaka-u.ac.jp.

10.1021/jp064327j CCC: $33.50
Published on Web 10/26/2006

TABLE 1: Properties of FTO/Ti Substrates with Titanium Films of Different Thicknesses

sputtering time (min)	Ti film thickness (nm)	sheet resistance (Ω/□)
bare FTO	0	9.1
Ti-0.5 min	3	8.7
Ti-5 min	32	8.8
Ti-20 min	123	8.7
Ti-30 min	185	9.3
Ti-40 min	246	9.2
Ti-60 min	370	5.5

10 Ω/□) using radio frequency magnetron sputtering equipment (SPW-025S, ULVAC). The sputtering target was a Ti disk of 99.99% purity (High Purity Chemicals Lab. Co. Ltd.) with a diameter of 100 mm. Different thicknesses of Ti were deposited onto FTO at a direct current power of 150 W under a working pressure of 1.0 Pa of Ar. The relationship between the Ti film thickness and the sputtering time is shown in Table 1. Sheet resistance of the FTO/Ti was measured by a Mitsubishi Kagaku MCP-T600 four-probe-type resistance meter, and the results are also summarized in Table 1.

Nanoporous TiO_2 electrodes were prepared on a transparent conductive substrate (Nippon Sheet Glass, SnO_2:F, 10 Ω/□) or FTO/Ti blocking substrates from the colloidal Nanoxide-T paste (Solaronix) by doctor-blade techniques. The films were annealed at 450 °C for 30 min in air. The resulting TiO_2 films (thicknesses of 5.5 ± 0.5 μm, measured by the profiler, Sloan Technology, Dektak 3) were cut into pieces and heated again at 110 °C for 15 min. Then, the electrodes were immersed in 3.0×10^{-4} M *cis*-bis(isothiocyanato)(2,2′-bipyridyl-4,4′-dicarboxylato)(2,2′-bipyridyl-4,4′-di-nonyl) ruthenium(II) (known as Z-907, Solaronix) in acetonitrile/*tert*-butyl alcohol (1:1) for 18 h. After being washed with acetonitrile, the sensitized electrode was covered with platinized conducting glass as a counter electrode. Typical areas of the electrodes were around to be 0.20 cm^2. The ionic liquid electrolyte for the DSCs was composed of 0.5 M *tert*-4-butylpyridine, 0.1 M LiI, and 0.2 M I_2 in 1-propyl-3-methylimidazolium iodide (PMImI) and 1-ethyl-3-methyl-imidazolium dicyanamide (EMIm-DCA) (2:1 PMImI/EMIm-DCA).

The photoelectrochemical properties of the DSCs were studied by recording the current−voltage ($I-V$) characteristics of the unsealed cell under illumination of AM 1.5 (1 sun, 100 mW/cm^2) using a solar simulator (Yamashita Denso, YSS-80). The data were obtained from the average of at least three examples. For the three-electrode electrochemical measurements in 0.1 M $LiClO_4$ and 1 mM ferrocene in acetonitrile, a 1 cm^2 area of the bare FTO and FTO/Ti glass, platinum foil, and Ag/AgCl served

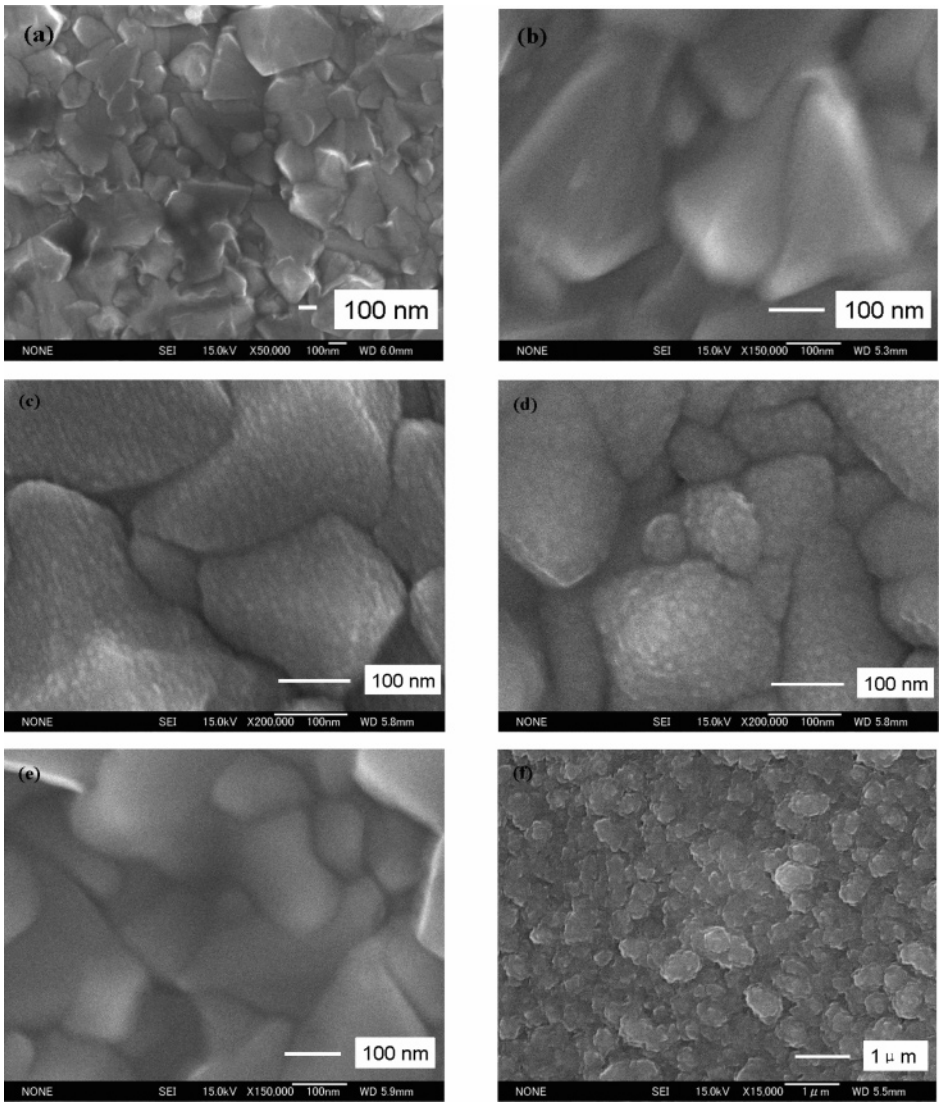

Figure 1. SEM micrographs of FTO glass and FTO/Ti substrates: (a) bare FTO substrate; (b−d) sputtering Ti for 5, 20, and 30 min; (e and f) sputtering 15 min and 3 h after calcinations at 450 °C.

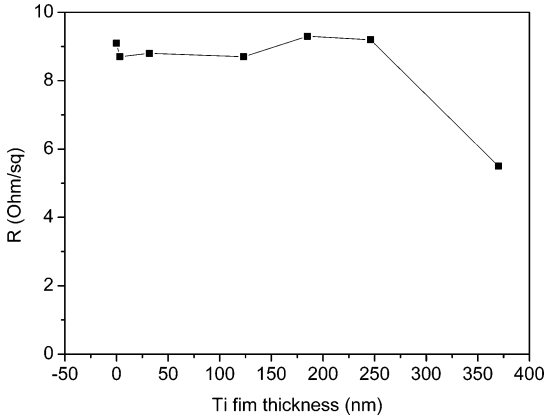

Figure 2. Relationship between the Ti thickness and the sheet resistance of FTO/Ti.

as the working, counter, and reference electrodes, respectively (BAS 100B/W electrochemical system). X-ray diffraction (XRD) patterns were obtained by a Rigaku RU-200B. The Ti film thickness was measured with a surface profilometer (Dektak 3 from Sloan Technology). The surface morphologies of bare FTO and FTO/Ti were analyzed using field emission scanning electron microscopy (FE-SEM, S-1400 Hitachi). The optical transmittance and absorption spectra measurements were collected with a JASCO (V-570) UV−vis−near-IR spectrophotometer at wavelengths from 300 to 1200 nm. The X-ray photoelectron spectroscoy (XPS) measurements were carried out with a Kratos AXIS 165 (Shimadzu) using a Mg Kα monochromatized X-ray source. The calcinations of the FTO/Ti substrate were carried out in ambient air. Etching processes were carried out using a 4 keV Ar^+ ion beam with an etching rate around 6 nm/min.

3. Results and Discussion

3.1. Surface Morphology of the FTO/Ti Substrate. Figure 1 shows the SEM surface morphologies of the bare FTO substrate and the FTO/Ti substrates. The bare FTO surface shows the characteristic morphology of tin oxide crystals (Figure 1a), whose particles are around 150−250 nm in size. After the first 5 min of sputtering, it is difficult to find other particles except SnO_2 on FTO. This might be due to the reaction of Ti atoms with FTO or diffusion to the boundaries of the FTO crystals. After 20 or 30 min of deposition of titanium, there are some small titanium particles about 10−15 nm in size on the FTO surface, as shown in Figures 1c and 1d. Along with the deposition time increasing to 1 h or more, it seems that the particle size does not change much, indicating no aggregation of the titanium nanoparticles. Figures 1e and 1f show the FTO/Ti substrate calcinations at 450 °C. For Ti-20 min, the rough surface changes to smooth with the disappearance of the small nanoparticles, which means that Ti metal might be oxidized to thin TiO_x film to an appreciable extent. However, in the case of Ti deposition for 3 h (thickness of Ti about 1 μm), 400−500 nm large particles exist on the surface. According to the XRD analysis, these large round particles were found to be titanium metal aggregation, although the surface might be covered with thin compact TiO_x.

3.2. Effect of Titanium Metal Film Thickness on Sheet Resistances of FTO. The variation of the sheet resistance of FTO after titanium deposition is exhibited in Figure 2. The sheet resistance (R_s) of FTO/Ti does not change too much with the Ti film thickness in the range of 0−200 nm, while it decreases from 9 to 5.5 Ω/□ with Ti film thickness up to 370 nm.

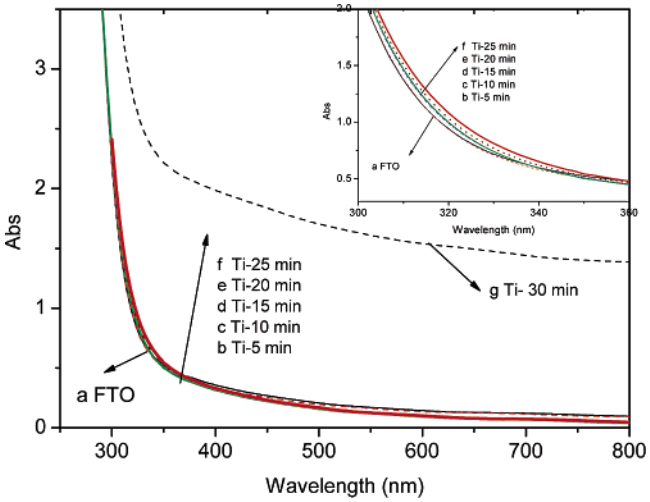

Figure 3. Absorption spectra of bare FTO and FTO/Ti substrates.

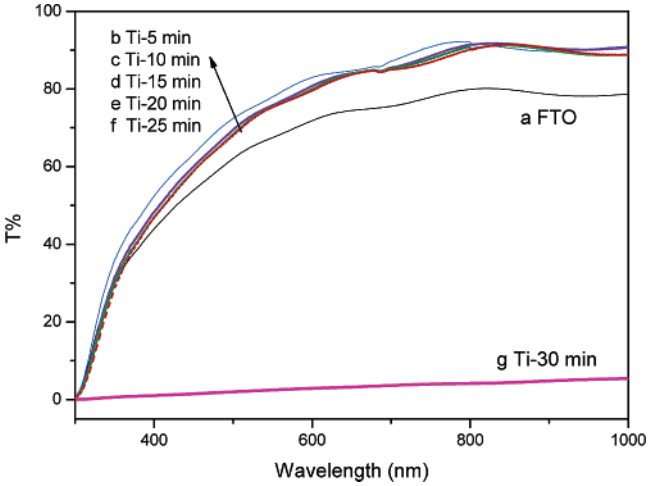

Figure 4. Optical transmittance of bare FTO and FTO/Ti substrates.

3.3. Optical Properties of FTO/Ti Substrates. Figure 3 presents the absorption spectra of the bare FTO substrate and different FTO/Ti substrates. The inset of Figure 3 shows magnification in the range of 300−400 nm. In comparison to bare FTO, the absorption edge is red-shifted after the deposition of thin Ti metal, which indicates that titanium may change the band gap of SnO_2 to some extent. Figure 4 shows the transmission spectra of the FTO/Ti substrates and comparison with the transmittance of bare FTO in the range from 300 to 1000 nm. For the bare FTO substrate, it gives an average transmittance of around 80% in the visible range while the FTO/Ti substrates exhibit a superior transmittance value of around 90% in the visible region when the thickness of titanium is less 150 nm (sputtering time less than 20 min). It is noted that the transparent FTO/Ti substrates change to opaque (black) with a poor transmittance value of lower than 5% once the sputtering time extends to 30 min. As far as DSCs fabrication is concerned, it is very important to deposit a thin titanium film on FTO.

3.4. XRD Patterns of FTO/Ti Substrates. Figure 5 shows the XRD patterns of the FTO and FTO/Ti substrates calcined at different temperatures. Because of the sensitivity, we prepared around 1 μm of titanium with 3 h of sputtering to obtain its clear XRD pattern. From this figure, in comparison to the bare FTO, there is a new peak appearing at 38.65° corresponding to the (110) plane of cubic β-Ti (JCPDS Card No. 44-1288) for FTO/Ti at room temperature. After the substrate was annealed at 450 °C, this peak shifts to 37.45° with a lower intensity partly

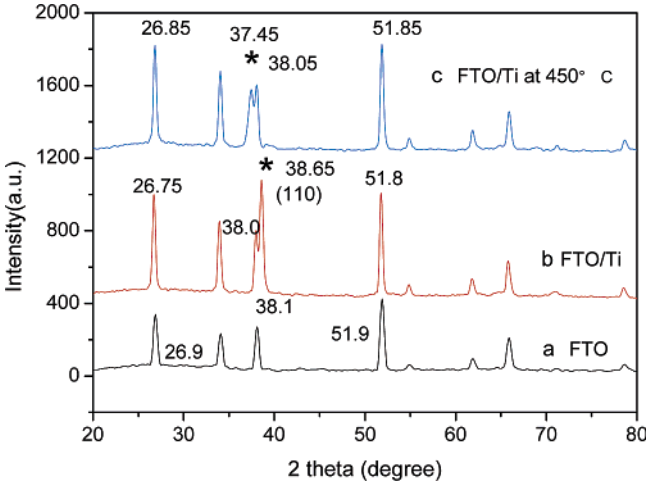

Figure 5. XRD patterns of FTO and FTO/Ti substrates before and after calcinations at 450 °C.

because of more TiO_x formation. Although there might be a trace amount of TiO_2 formed at the surface of titanium, it is difficult to detect such a new phase with the XRD technique. A more detailed analysis based on XPS is in the following section.

3.5. XPS Analysis of the FTO/Ti Substrate. XPS measurements were employed to examine the valences of the Ti species and their interaction with FTO. The examined samples are Ti-20 min substrates. Figures 6 and 7 present the changes in the XPS spectrum of O 1s, Ti 2p, and Sn 3d of FTO/Ti at different etching times. For detail analysis, the curve fitting and deconvolution of O 1s and Ti 2p regions in the XPS spectra are also shown in these figures.

Before the substrate was etched, the O 1s feature shown in Figure 6 is composed of three peaks. One is at 530.3.eV, which corresponds to oxygen in Ti−O groups. The second strongest peak is at 532.5 eV, which corresponds to oxygen in OH^- groups.[36] The smaller peak with a higher binding energy of 535.6 eV is assigned to chemisorbed oxygen and/or oxygen[37] on the remaining FTO/Ti surface. In comparison to the spectra before etching (etching 0 min), the intensity of the O 1s peak of OH^- decreased with the peaks of chemisorbed oxygen disappearing and the absorption of oxygen always occurring on the surface after 3 min of etching. However, a new peak at 537.1 eV formed, belonging to the O K-edge band. The O K-edge in the range of ~535−546 eV is due to transitions from oxygen 1s to 2p states that hybridized with Ti 4s and 4p states.[38] Such an O K-edge is very common in Ti-containing minerals such as Ba_2TiO_4 or titanium silicate glasses.[38] In addition, this O K-edge is still observable after etching 25 min.

Figures 7a and 7b show the changes of the XPS spectra of Sn 3d and Ti 2p during etching. The primary peak at 486.8 eV is Sn^{4+} because SnO_2 is the main part of FTO. Interestingly, in the profile of Sn 3d, a new component at a lower binding energy (484.7 eV) characteristic of Sn^0 is observed while disappearing after 20 min of etching for detection into the deep FTO layer. Since oxygen is not present in the gas phase during the Ti film growth, we need think about the reduction reactions with tin oxide by Ti. More detailed analysis was reported by Gouttebaron et al.[39] The valence change of Sn and the observation of O K-edge band in XPS spectra suggest that titanium should interact strongly with the FTO layer.

Furthermore, the curve fitting and deconvolution of the Ti 2p regions of the XPS spectra are also shown in Figures 7c and 7d. Before the substrate was etched, only the Ti^{4+} signal is

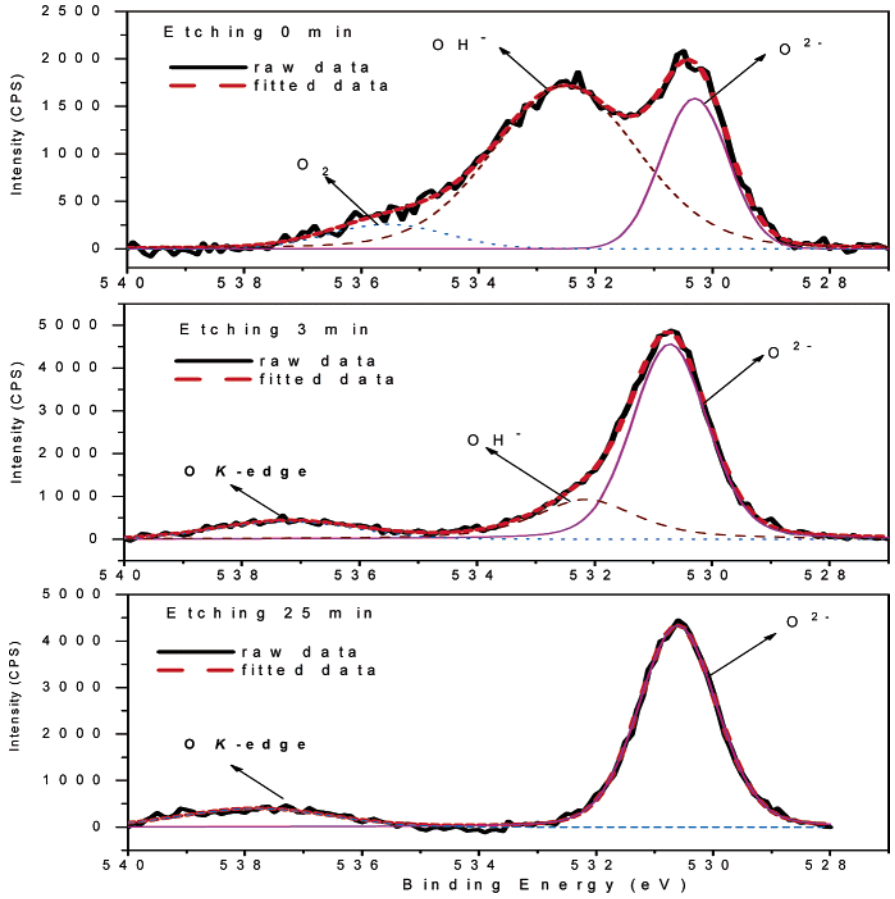

Figure 6. XPS spectra and curve fits for of O 1s during Ar^+ etching.

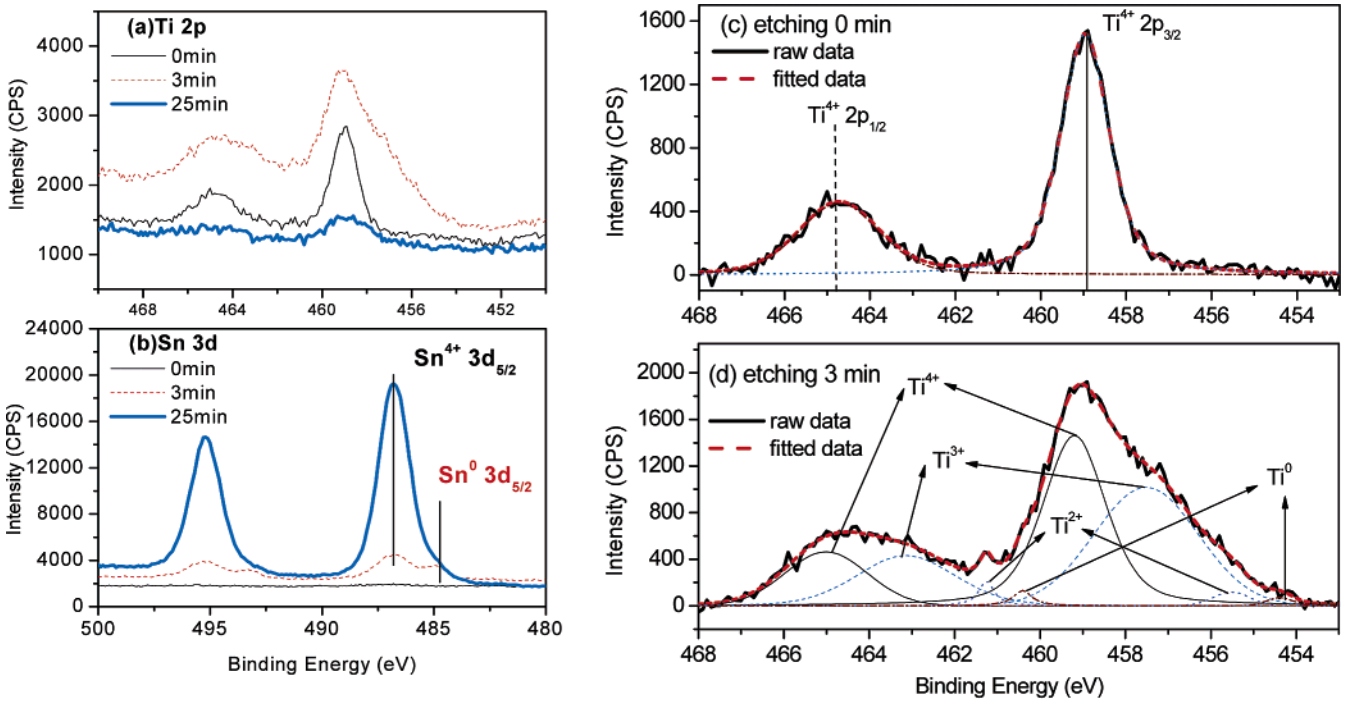

Figure 7. XPS spectra of Ti 2p and Sn 3d peaks of the FTO/Ti after different etching durations. The etching times are 0, 3, and 20 min: (a) Ti 2p; (b) Sn 3d and the spectra of Ti 2p peaks fitted (c) before etching (etching time 0 min) and (d) after etching for 3 min.

detectable on the surface, indicating that thin TiO_2 formed on the FTO/Ti surface. Along with the etching, signals containing peaks of Ti^{4+} (465.0 and 459.2 eV), Ti^{3+} (463.1 and 457.5 eV), Ti^{2+} (461.3 and 455.5 eV), and Ti^0 (454.4 and 460.4 eV) are observable. Meanwhile, Ti^{4+} and Ti^{3+} are the majority in the TiO_x layer along with less than 5% of Ti^{2+} and Ti^0. Although the distribution of these Ti species is different than that in an earlier report[39] with in situ analysis, in our case, a minority of metallic Ti among the total distribution of Ti species in FTO/Ti is reasonable for the exposure to air before examination. Therefore, Ti modified FTO should be noted as FTO/TiO_x. Moreover, we found that the final form of FTO/Ti (after calcination at 450 °C for 30 min) maintains its original state except that the trace amount of Ti^0 disappeared. (See the deconvolution of the Ti 2p regions of the XPS spectra in Figure S1 of the Supporting Information.)

As proposed by Gouttebaron et al.,[39] the growth of Ti on FTO with a deposition rate of >0.05 nm/s should be a metastable version of the Frank van der Merwe mode or a pseudo-FM mode. Taking the consideration that the Ti deposition rate in our experimental conditions (Table 1) is around 0.1 nm/s, Ti should give a homogeneous coverage on FTO. Such an imaginable mechanism is verified by cyclic voltammetric behaviors in the following section.

3.6. Performance of DSCs Based on FTO and FTO/Ti Substrates. Figure 8 shows the $J-V$ characteristics of DSCs based on the novel solar cell and that of the reference at AM 1.5 irradiation of 100 mW/cm^2. Their parameters are listed in Table 2. Without a blocking layer, the cell shows only J_{sc} = 7.9 mA/cm^2, V_{oc} = 663 mV, and ff = 0.66, corresponding to a conversion efficiency of 3.5%. After the deposition of thin TiO_x at the interface of FTO/nano-TiO_2, these devices give a great improvement of $V_{oc}$of about 30−50 mV and a superior fill factor with a better conversion efficiency. Especially in the case of Ti-15 min (the number represents the sputtering time), this device gives the highest improvement of V_{oc} of about 50 mV and a better fill factor with some increase of J_{sc}, finally resulting in a 4.4% energy conversion efficiency, which is 20% higher

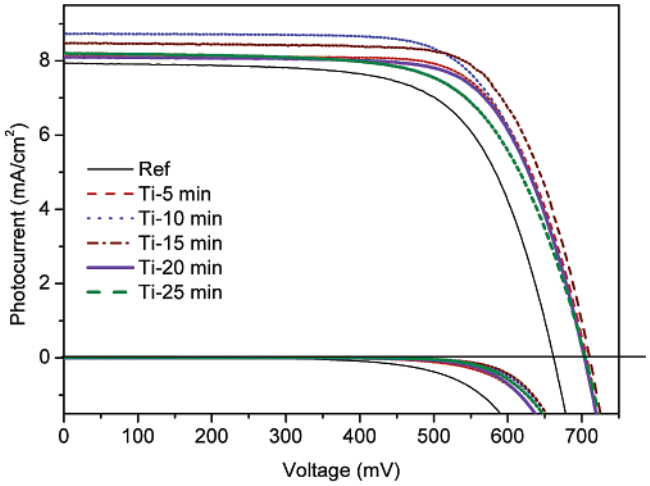

Figure 8. $J-V$ curves of DSCs with 5.5-μm-thick nano-TiO_2 layer on FTO and FTO/Ti substrates under AM 1.5, 100 mW/cm^2 illumination.

TABLE 2: Performance of DSCs Using FTO/Ti Substrates Composed with Different Ti Sputtering Times

Ti sputtering time (min)	Ti thickness (nm)	V_{oc} (mV)	J_{sc} (mA/cm^2)	ff	η (%)
Ti-0	0	663 ± 5	7.9 ± 0.2	0.66 ± 0.01	3.5 ± 0.1
Ti− 5min	31	702 ± 10	8.1 ± 0.4	0.72 ± 0.03	4.1 ± 0.1
Ti-10 min	62	704 ± 4	8.7 ± 0.2	0.69 ± 0.01	4.2 ± 0.1
Ti-15 min	93	711 ± 2	8.4 ± 0.2	0.73 ± 0.01	4.4 ± 0.1
Ti-20min	123	690 ± 2	8.3 ± 0.2	0.73 ± 0.01	4.1 ± 0.1
Ti-25min	154	705 ± 5	8.5 ± 0.3	0.64 ± 0.05	3.80 ± 0.1
Ti-30min	185	436 ± 20	0.1 ± 0.1	0.32 ± 0.05	0.016 ± 0.1

than that of the nonblocked electrode. Along with an increase in sputtering time, Ti-25 min gives a lower ff of about 0.64 with a 3.8% of conversion efficiency. However, in the case of Ti-30 min (thickness over 180 nm), the cell exhibits very poor performance due to the loss of visible light by the opaque, black FTO/Ti substrate. As shown in Figure 4, the *T*% of FTO/Ti-30

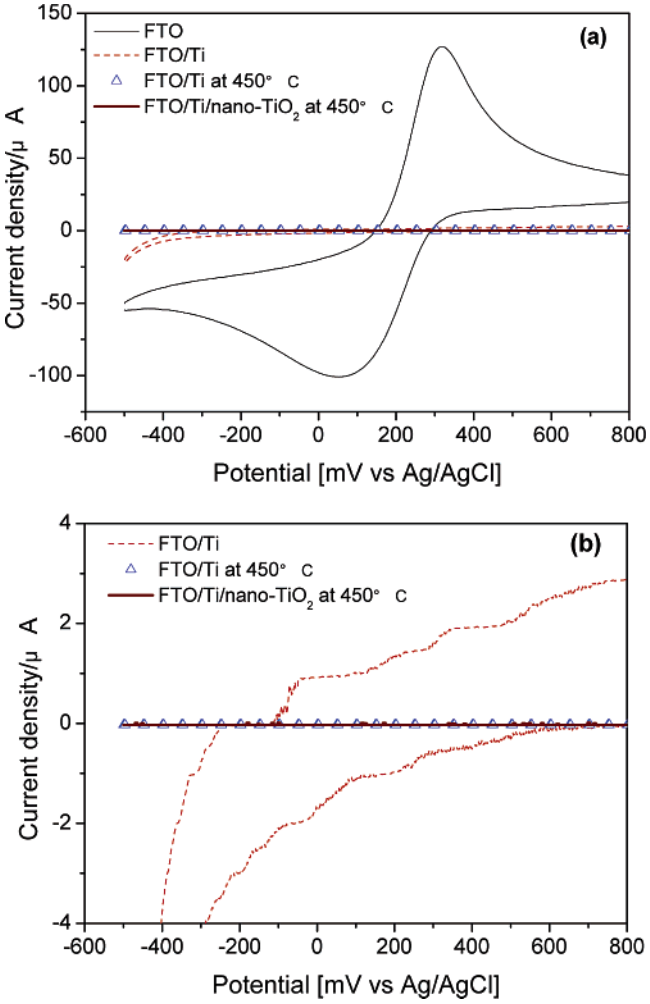

Figure 9. Cyclic voltammogramms of FTO and FTO/Ti substrates (electrodes) ata scan rate of 100 mV/s; (a) FTO, FTO/Ti, and a FTO/Ti/nano-TiO_2 electrode after calcinations at 450 °C; (b) magnification of part a.

min in the visible region is lower than 10%. Therefore, the 30 min deposition is the threshold for *T*% in the titanium blocking system. As a whole most of the Ti blocking electrodes exhibit a higher J_{sc} compared to that of the reference due to their superior transmittance over 85% averaged in the visible region. In comparison to the TiO_2 compact layer[25] formed by a common spray pyrolysis method, the advantage of the titanium blocking substrate is that it can improve not only ff and V_{oc} but also J_{sc} in ionic liquid DSCs.

The improved ff might be due to the improved electrical contact at the FTO/nano-TiO_2 interface. Since the rutile structure of SnO_2 (FTO) induced the formation of rutile TiO_2,[40,41] TiO_x should contain rutile TiO_2 and match well with the nano-TiO_2 layer and FTO layer, leading to a good electron transporting process at the interfaces. Therefore, a FTO/TiO_x/nano-TiO_2 electrode can lower electron loss at FTO/electrolyte and FTO/nano-TiO_2 interfaces, which means that it can enhance the electron collection efficiency at FTO, giving an improvement of V_{oc} for the accumulation of injected electrons.

It is noted that we just investigate the effect of the blocking layer on an ionic liquid electrolyte based on thin layer TiO_2 in this paper. Although the conversion efficiency is not very high at this moment, it is expectable to obtain a better performance after employing a scattering layer and a superior dye such as N-719.

3.7. Electrochemical Characterization. Figure 9 shows cyclic voltammetric curves of the ferrocene (Fc/Fc^+) redox reaction at various electrodes. The redox current of bare FTO is the highest at around 120 μA compared to those Ti-modified FTO substrates. In the case of the Ti-20 min electrode (substrate), a few microamperes of redox current indicates the surface of FTO can be well covered with TiO_x. Interestingly, after being annealed at 450 °C, this substrate shows even the lowest redox current of around 60 nA. And even in the case of FTO/Ti/nano-TiO_2, it still maintains the lowest redox current in the redox reaction (Figure 9b). In our previous study,[42] high-temperature calcination of a binder-containing nano-TiO_2 paste will damage the compact TiO_2 layer (obtained by sputtering TiO_2 target), leading to the increase of the redox current to the 10 μA level. To some extent, the blocking layer obtained by Ti sputtering is superior to the TiO_2 blocking layer prepared by spray pyrolysis or sputtering of TiO_2.

With this evidence, we can conclude that Ti/TiO_x can perfectly suppress electron leakage at the interfaces of FTO/nano-TiO_2 and FTO/electrolyte, with the reasons as follows:

(1) The TiO_x layer is denser than TiO_2 because of their different lattice structures.

(2) Titanium is very reactive with SnO_2 in FTO, which will be favorable for tight attachment to the FTO layer at thermal treatment during fabrication of DSCs.

In our previous study,[43] we reported the development of a substrate as TiO_2/Ag/TiO_2 with good performance in DSCs. Our novel substrate FTO/TiO_x can be extended to develop other metal substrates such as metal/TiO_x as flexible DSCs for future applications.

Conclusions

Deposition of thin TiO_x from a Ti metal target has been developed as a new type of blocking material at the FTO/nano-TiO_2 interface. Such an electrode can improve V_{oc} and ff without lowering J_{sc} in ionic-liquid-based solar cells with 15−20% improvement of conversion efficiency. The advantage of such an electrode is that it can perfectly suppress electron leakage at the FTO/nano-TiO_2 interface and improve the transmittance of the FTO substrate to some extent. The cyclic voltammetric behaviors reveal that the effective TiO_x blocking layer plays an important role in unidirectional electron transport at interfaces in DSCs through perfect morphological control.

Acknowledgment. This research was supported by the New Energy and Industrial Technology Development Organization under the Ministry of Economy, Trade and Industry.

Supporting Information Available: Deconvolution of Ti 2p regions XPS spectra for FTO/Ti substrate after thermal treatment. This material is available free of charge via the Internet at http://pubs.acs.org.

References and Notes

(1) Wang, P.; Wenger, B.; Humphry-Baker, R.; Moser, J.-E.; Teuscher, J.; Kantlehner, W.; Mezger, J.; Stoyanov, E. V.; Zakeeruddin, S. M.; Grätzel, M. *J. Am. Chem. Soc.* **2005**, *127*, 6850.

(2) Wang, P.; Zakeeruddin, S. M.; Humphry-Baker, R.; Grätzel, M. *Chem. Mater.* **2004**, *16*, 2694.

(3) Matsumoto, H.; Matsuda, T.; Tsuda, T.; Hagiwara, R.; Ito, Y.; Miyazaki, Y. *Chem. Lett.* **2001**, *30*, 26.

(4) Yamanaka, N.; Kawano, R.; Kubo, W.; Kitamura, T.; Wada, Y.; Watanabe, M.; Yanagida, S. *Chem. Commun.* **2005**, 740.

(5) Hagiwara, R.; Ito, Y. *J. Fluorine Chem.* **2000**, *105*, 221.

(6) Welton, T. *Chem. Rev.* **1999**, *99*, 2071.

(7) McEwen, A. B.; Ngo, H. L.; LeCompte, K.; Goldman, J. L. *J. Electrochem. Soc.* **1999**, *146*, 1687.

(8) Wang, S.; Liu, Y.; Huang, X.; Yu, G.; Zhu D. *J. Phys. Chem. B* **2003**, *107*, 12639.

(9) Krüger, J.; Bach, U.; Grätzl, M. *Adv. Mater*. **2000**, *12*, 447.

(10) Ho, P. K. H.; Granström, M.; Friend, R. H.; Greenham, N. C. *Adv. Mater*. **1998**, *10*, 769.

(11) Choi, B.; Rhee, J.; Lee, H. H. *Appl. Phys. Lett.* **2001**, *79*, 2109.

(12) Campbell, I. H.; Kress, J. D.; Martin, R. L.; Smith, D. L.; Barashkov, N. N.; Ferraris, J. P. *Appl. Phys. Lett.* **1997**, *71*, 3528.

(13) Appleyard, S. F. J.; Day, S. R.; Pickford, R. D.; Wills, M. R. *J. Mater. Chem.* **2000**, *10*, 169.

(14) Morgado, J.; Charas, A.; Barbagallo, N. *Appl. Phys. Lett.* **2002**, *81*, 933.

(15) Levy, B.; Liu, W.; Gilbert, S. E. *J. Phys. Chem. B* **1997**, *101*, 1810.

(16) Zaban, A.; Meier, A.; Gregg, B. A. *J. Phys. Chem. B* **1997**, *101*, 7985.

(17) Pichot, F.; Gregg, B. A. *J. Phys. Chem. B* **2000**, *104*, 6.

(18) Cahen, D.; Hodes, G.; Grätzel, M.; Guillemoles, J. F.; Riess, I. *J. Phys. Chem. B* **2000**, *104*, 2053.

(19) Lagemaat, J.; Park, N.-G.; Frank, A. J. *J. Phys. Chem. B* **2000**, *104*, 2044.

(20) Fabregat-Santiago, F.; Garcia-Belmonte, G.; Bisquert, J.; Bogdanoff, P.; Zaban, A. *J. Electrochem. Soc.* **2003**, *150*, E293.

(21) Kavan, L.; Grätzel, M. *Electrochim. Acta* **1995**, *40*, 643.

(22) Gregg, B. A.; Pichot, F.; Ferrere, S.; Fields, C. L. *J. Phys. Chem. B* **2001**, *105*, 1422.

(23) Peng, B.; Jungmann, G.; Jäger, C.; Haarer, D.; Schmidt, H. W.; Thelakkat, M. *Coord. Chem. Rev.* **2004**, *248*, 1479.

(24) Ito, S.; Liska, P.; Comte, P.; Charvet, R.; Péchy, P.; Bach, U.; Schmidt-Mende, L.; Zakeeruddin, S. M.; Kay, A.; Nazeeruddin, M. K.; Grätzel, M. *Chem. Commun.* **2005**, 4351.

(25) Hore, S.; Kern, R. *Appl. Phys. Lett.* **2005**, *87*, 263504.

(26) Hart J. N.; Menzies D.; Cheng Y. B.; Simon G. P.; Spiccia L. *C. R. Chim*. **2006,** *9***,** 622.

(27) Kang T. S.; Moon S. H.; Kim K. J. *J. Electrochem. Soc.* **2002**, *149*, E155.

(28) Han H. W.; Zhao X. Z.; Liu J. *J. Electrochem. Soc.* **2005**, *152*, A164.

(29) Cameron, P. J.; Peter, L. M. *J. Phys. Chem. B* **2003**, *107*, 14397.

(30) Cameron, P. J.; Peter, L. M.; Hore, S. *J. Phys. Chem. B* **2005**, *109*, 930.

(31) Cameron, P. J.; Peter, L. M. *J. Phys. Chem. B* **2005**, *109*, 7392.

(32) Xia, J. B.; Masaki, N.; Jiang, K. J.; Wada, Y.; Yanagida, S. *Chem. Lett.* **2006**, *35*, 252.

(33) Xia, J. B.; Masaki, N.; Jiang, K. J.; Wada, Y.; Yanagida, S. *Chem. Commun.*, in press, doi: 10.1039/b610588b.

(34) Kron, G.; Rau, U.; Werner, J. H. *J. Phys. Chem. B* **2003**, *107*, 13258.

(35) Chappel, S.; Grinis, L.; Ofir, A.; Zaban, A. *J. Phys. Chem. B* **2005**, *109*, 1643.

(36) Olsson, C.-O. A.; Landolt, D. *Corros. Sci.* **2004**, *46*, 213.

(37) Biniak, S.; Szymanski G.; Siedlewski, J.; Swiatkowski, A. *Carbon* **1997**, *35*, 1799.

(38) Henderson, G. S.; Liu, X.-Y.; Fleet, M. E. *Mineral. Mag.* **2003**, *67*, 597.

(39) Godfroid, T.; Gouttebaron, R.; Dauchot, J. P.; Leclere, Ph.; Lazzaroni, R.; Hecq, M. *Thin Sold Films* **2003**, *437*, 57.

(40) Lindgren, T.; Mwabora, J. M.; Avendano, E.; Jansson, J.; Hoel, A.; Granqvist, C.-G.; Lindquist, S.-E. *J. Phys. Chem. B* **2003**, *107*, 5709.

(41) Ferreira da Silva, A.; Pepe, I.; Silva Brasil C. S.; David, D. G..F.; Silva, E. F.; Persson, J. C.; Lindgren, T.; Almeida, J. S.; Moyses Araujo, C.; Ahuja, R. *Phys. Status Solidi C* **2004,** *1*, S241.

(42) Saito, Y. Ph.D. Thesis, Osaka University, 2004.

(43) Ito, S.; Takeuchi, T.; Katayama, T.; Sugiyama, M.; Matsuda, M.; Kitamura, T.; Wada, Y.; Yanagida, S. *Chem. Mater*. **2003**, *15*, 2824.